 DOI: 10.1002/masy.200751414

Density Functional Calculations for Electronic and Steric Effects of Ethyl Benzoate on Various Ti Species in $MgCl_2$-Supported Ziegler-Natta Catalysts

*Toshiaki Taniike, Minoru Terano**

Summary: Possible coadsorption states of Ti mononuclear species and ethyl benzoate (EB) and their interaction on $MgCl_2$ (110) and (100) surfaces were investigated with periodic density functional calculations in order to obtain the microscopic understanding about how EB affects the steric and electronic natures of the Ti species. EB was unlikely to be attached to the $TiCl_4$ species on both the $MgCl_2$ (110) and (100) surfaces. The coadsorption of EB at Mg^{2+} ions near the Ti species was as favorable as the separate adsorption, which implied the random placement of these adsorbants in the final catalyst. The charge redistributions upon coadsorption among the Ti species, EB and the support were found to be dependent on the surface structures: the electron density of the Ti speceies was rather decreased by the coadsorption on the (100) surface, while that of the Ti species was enhanced due to the support-mediated electron transfer from EB on the (110) surface. It was suggested that the presence of EB close to the Ti species should generate donor-related active sites selectively on the (110) surface.

Keywords: coadsorption of ethyl benzoate and Ti species; computer modeling; density functional calculation; Ziegler-Natta polymerization

Introduction

Heterogeneous Ziegler-Natta catalysts for stereoselective polymerization of propylene are one of the most valuable industrial catalysts, owing to the broad versatility of the resulting polypropylene. The Ziegler-Natta catalysts are basically composed of $MgCl_2$ as a catalytic support, $TiCl_4$ as an active site precurser, and internal donors that are essential to drastically improve the stereospecifity of the catalysts. Alkyl aluminum reducing or alkylating agents are added to activate the catalysts for polymerization, with an adequate type of external donors mainly to further improve the stereospecifity.

Although the above-mentioned catalyst components have been unchanged since the discovery of the first donor, ethyl benzoate (EB),[1] new types of donors have continuously improved catalytic properties such as stereospecifity, activity, hydrogen response and molecular weight distribution. In order to reach a further stage, it is highly desired to know the roles of the donors in making the catalyst precursor and in polymerization at the molecular level. At present, there have been several proposals for the donors' roles, which may conflict or coexist with each other.[2–10]

The internal donors have been proposed to play the following roles,

i) activate the $MgCl_2$ support during the catalyst preparation,
ii) selectively block the non-stereoselective (110) surface to increase the isospecific Ti dinuclear species on the stereoselective (100) surface,[5]

School of Materials Science, Japan Advanced Institute of Science and Technology, 1-1 Asahidai, Tatsunokuchi, Ishikawa, 923-1211, Japan
Fax: (+81)761 51 1625;
E-mail: terano@jaist.ac.jp

iii) coadsorb with Ti species to transform aspecific sites into isospecific sites by their bulkiness.[4,6,7]

The external donors have been considered to make complexes with alkyl aluminum compounds, and the following roles have been claimed,

iv) selectively activate isospecific sites or deactivate aspecific sites,

v) occupy the vacant positions resulting from the extraction of the internal donors to keep the bulkiness around the Ti species.

Although these roles are a kind of consensus based on the historically collected corroborations, it is still unclear when and how each role affect the catalytic properties at the molecular level, and why only the limited Lewis bases with specific molecular structures work as an effective donor. The difficulties in clarifying these questions come from the competition of the multiple roles of the donors, heterogeneous and multi-components nature of the catalyst system, and the lack of in-site characterizations.

Theoretical approaches are nowadays regarded as one of the most effective tools to overcome the difficulties for clarifying the roles of the donors. Cavallo et al. calculated the adsorption of 1,3-diether with different substituents on clean $MgCl_2$ (110) and (100) surfaces using the semi-empirical AM1 method[11] They concluded that the preference of the 1,3-diether to the (110) surface correlated with the experimentally obtained isotacticty of the polypropylene, which supported their proposal that the non-stereoregular surface was (110).[5] The same trend was also found by L. Barino et al. using the classical molecular mechanics.[12] The dibutyl phthalate (DBP) adsorption in the presence of mononuclear Ti species was studied by Boero et al. within the framework of the Car-Parrinello molecular dynamics, which found the preference of DBP to the $MgCl_2$ (100) surface rather than (110)[13] on the contrary to the proposal by Busico et al.[5] Seth et al. examined the effect of the direct adsorption of tetrahydrofuran (THF) onto mononuclear Ti active species on ethylene polymerization using $MgCl_2$ (110) and (104) clusters with gradient corrected density functional calculations.[14] They showed that the direct adsorption of THF hindered the chain transfer reaction more than the ethylene insertion, leading to higher molecular weight of polyethylene. Finally, Yao et al. suggested using classical simulations that the interaction energy between a series of silane external donors and $TiCl_4$-TEA complex on the $MgCl_2$ support should be a key factor to decide the performance of the external donors.[15]

In spite of these works, comprehensive simulations with the first-principle accuracy are still rare. Especially, for the coadsorption role of the donors, there have been few first-principle calculations using a sufficient size of the support, although the importance of the coadsorption was obviously stressed in the (modified) 3-sites model by Busico et al.[6] and Terano et al.[7] as well as in the chain-end analysis of Sacchi et al.[4] In this article, periodic density functional calculations were conducted in order to clarify plausible coadsorption states and interaction between ethyl benzoate (EB) and $TiCl_x$ ($x = 3,4$) mononuclear species on single crystal $MgCl_2$ (110) and (100) surfaces, as a series of studies about the donors' roles.

Methods

The density functional calculations were based on the exchange-correlation functional of Perdew, Becke and Ernzerh (PBE)[16] at the level of the generalized gradient approximation.[17] The basis set was the double-numerical basis plus polarization functions (DNP) combined with the effective core potentials of Dolg et al.[18] The other numerical parameters including the convergence tolerances, density of the integration grid and real-space cutoff radius were set to those of the ''medium accuracy'' within the density functional code, DMol3[19] (refer to Ref. [20] for further

details). Higher accuracy did not introduce any notable improvement of the results. The spin polarization was considered for the systems including a Ti^{3+} ion. The charge analysis was based on the Hirshfeld method, appropriate for the numerical basis set.[21]

The $MgCl_2$ bulk was assumed to have the most stable α crystalline phase with the lattice constants fixed at the experimental values, 0.3636 and 1.7666 nm. The slab method was used for the boundary condition, inserting 0.15 nm of the vacuum layer between the two neighboring slabs. The most stable (001) $MgCl_2$ plane was known inactive for the adsorption of $TiCl_4$ without reduction[22] due to the lack of coordinatively unsaturated Mg^{2+} ions. Therefore the (110) and (100) planes were employed as the representative catalyst surfaces, which expose 4-fold and 5-fold coordinated Mg^{2+} ions, respectively. To obtain the fully convergent behaviour in terms of the slab thickness is a quite difficult task in highly ionic systems, we took 6 atomic layers for the (110) slab and 14 atomic layers for the (100) slab owing to the balanced performance. As will be stated later, the extent of the convergence was lower for the non-neutral (100) surface even with 14 atomic layers. For the adsorption of $TiCl_x$ ($x = 3,4$) and EB, a p(2x2) unit cell having 24 $MgCl_2$ units was used for the (110) surface and a p(3x1) unit cell having 36 $MgCl_2$ units was for the (100) surface. $1 \times 1 \times 1$ and $2 \times 1 \times 1$ k points were respectively applied to the p(2x2) (110) and p(3x1) (100) surfaces, ensuring the convergent adsorption energies. During geometry optimization, the bottomo two atomic layers were fixed at the bulk position.

Results and Discussion

Possible adsorption states of $TiCl_4$ and $TiCl_3$ mononuclear species were investigated on the $MgCl_2$ (110) and (100) surfaces. Three adsorption states for $TiCl_4$ have been proposed,[23,24] shown in Figure 1a-c: a) 6-fold coordinated epitactic species, where the Ti species bridges two adjacent 4-fold coordinated Mg^{2+} ions within one layer of $MgCl_2$ (6f intra-layer $TiCl_4$), b) 6-fold coordinated non-epitactic species, which bridges two Mg^{2+} across two $MgCl_2$ layers (6f inter-layer $TiCl_4$), and c) 5-fold coordinated species, proposed by Parrinello et al. as a potential precursor (5f $TiCl_4$).[24]

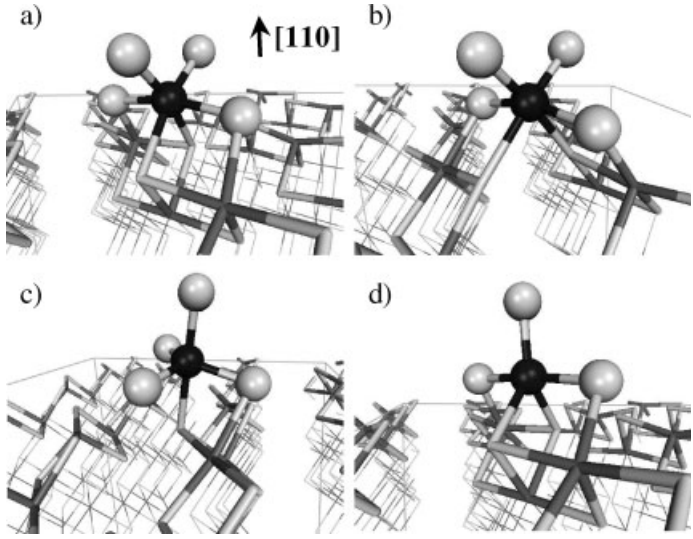

Figure 1.
Various $TiCl_4$ and $TiCl_3$ mononuclear species on the $MgCl_2$ (110) surface. a) 6f intra-layer $TiCl_4$, b) 6f inter-layer $TiCl_4$, c) 5f $TiCl_4$ and d) 5f intra-layer $TiCl_3$. Black: Ti, dark grays: Mg, and light gray: Cl.

In our calculations, the most stable species was the 6f intra-layer species with the adsorption energy (E_{ad}) of −19.77 kcal/mol, while E_{ad} of the 6f iner-layer species was −11.61 kcal/mol. As was pointed out in previous calculations,[23] 5f species had only −4.42 kcal/mol of E_{ad} (actually, this species was transformed into the 6f intra-layer species in the course of geometry optimization when the slab thickness was increased to 10 atomic layers). Namely, the breakment of O_h symmetry required a large energetic penalty. Three Ti mononuclear species were obtained by removing one terminal Cl^- ion from the corresponding $TiCl_4$ species: 5f intra-layer (Figure 1d), 5f inter-layer, and 4f $TiCl_3$ species (in the former two species, the remaining terminal ion pointed towards the surface normal). Their E_{ad} were respectively −33.82, −32.13, and −22.96 kcal/mol, where the difference of E_{ad} among the three states was decreased from the case of $TiCl_4$. On the (100) surface, only 4-fold coordinated bridging $TiCl_4$ (Figure 2a) was found with −11.43 kcal/mol of E_{ad}.[23] On the other hand, two bridging states (Figure 2b-c) and one monodentate state (Fig. 2d) were obtained for $TiCl_3$, whose E_{ad} were calculated to be −30.87, −24.85 and −20.83 kcal/mol, respectively.

As is summarized in Table 1 (only for the most stable species on each surface), it is obvious that E_{ad} of the Ti species are larger on the (110) surface than on the (100) surface, and that the charge transfer from the support to the Ti species are largely depressed on the (100) surface, especially for $TiCl_3$.

For the adsorption of EB, only monodentate structures with O of C=O bound to Mg^{2+} had potential energy minima, while any bidentate structures[25] with O–C=O bound to Mg^{2+} were transformed into monodentate forms during geometry optimization. On the (110) surface, the most stable EB (Figure 3a) made its molecular plane almost vertical to the surface Cl-Mg-Cl unit, and its E_{ad} was −29.82 kcal/mol.

It is notable that the rotation of EB around the C=O axis accompanied slight energetic change on the (110) surface unless the molecular plane became parallel to the Cl–Mg–Cl unit. On the (100) surface, there were found two monodentate states (Figure 3b) with similar E_{ad} (*ca.* −30 kcal/mol). The two states were different in the orientation of the molecular plane: paralell

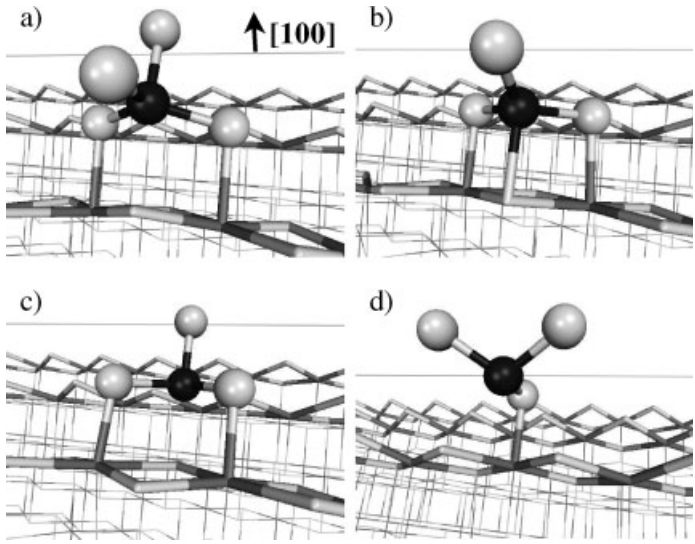

Figure 2.
Various $TiCl_4$ and $TiCl_3$ mononuclear species on the $MgCl_2$ (100) surface. a) bridging $TiCl_4$, b)-c) bridging $TiCl_3$, and c) monodentate $TiCl_3$.

Table 1.
The most stable Ti species and EB on the $MgCl_2$ (110) and (100) surfaces.

$MgCl_2$ surface	species	E_{ad}/kcal · mol^{-1}	charge		C=O/nm
			$TiCl_x$ or EB	$MgCl_2$	
(110)	$TiCl_4$	−19.78	−0.122	0.125	–
	$TiCl_3$	−33.81	−0.153	0.156	–
	EB	−29.83	−0.170	0.173	0.1238
(100)	$TiCl_4$	−12.95	−0.073	0.076	–
	$TiCl_3$	−30.86	−0.002	0.006	–
	$EB_{//}$ [a)]	−30.54	−0.132	0.137	0.1241
	$EB_{\perp}$ [a)]	−29.59	−0.110	0.117	0.1246

[a)] $EB_{//}$ and $EB_{\perp}$ mean the adsorption states of EB with its molecular axis parallel and perpendicular to the $MgCl_2$ layer, respectively.

or perpendicular to the $MgCl_2$ layer. With our unit cells, the adsorption energies of EB became similar on the two surfaces, but it was due to incomplete convergence for the slab thickness of the (100) surface. Increasing the slab thickness for the (100) surface from 14 to 20 atomic layers weakened the EB-surface interaction by 3.26 kcal/mol. As in the case of the Ti species, the charge transfer from EB to the support is larger for the (110) surface (Table 1).

Next, various coadsorption states of the Ti species and EB were examined on both the (110) and (100) surfaces, to know how they interact with each other on the catalyst support. We assumed that the Ti species had the most stable structure on the (110) surface, because EB was rotationally flexibile enough around the C=O axis to release steric repulsion with the adjacent Ti species. In addition, both the Ti species and EB could keep the most stable structures on the (100) surface even when they coexisted close to each other. The only exceptional case was the direct attachment of EB onto the $TiCl_4$ species, where structural transformation was inevitable to offer one vacant site for EB.

Three coadsorption states of the $TiCl_4$ mononuclear species with EB were shown in Figure 4a-c as typical examples on the (110) surface:

a) direct attachment of EB onto the $TiCl_4$ species, which required the structural transformation of $TiCl_4$ from 6f intralayer to 5f species,
b) adsorption of EB at the 5-fold coordinated Mg^{2+} ion binding the $TiCl_4$ species, where EB coordinated to the

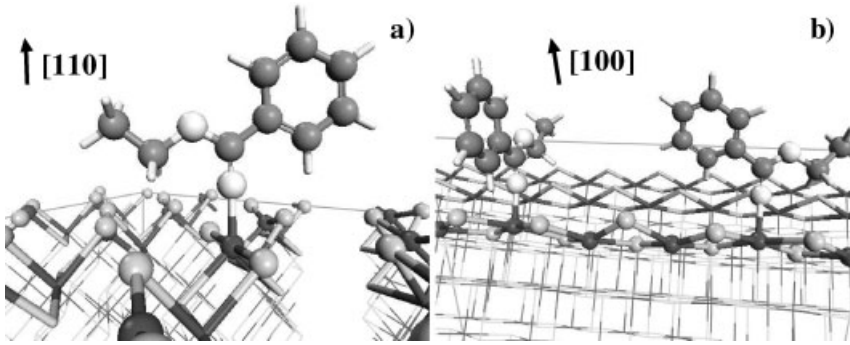

Figure 3.
The most stable structures of EB on the $MgCl_2$ a) (110) and b) (100) surfaces. Note that the two structures on the (100) surface with similar stability are differrent in the orientation of the molecular plane. Dark grays: Mg, light gray: Cl, gray: C, white balls: O, and white sticks: H.

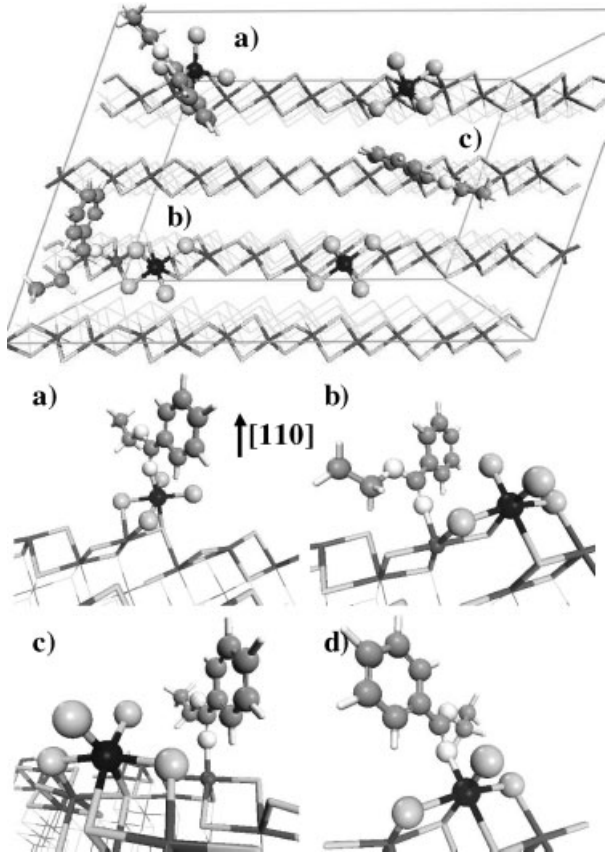

Figure 4.
Typical coadsorption states of EB and $TiCl_4$ ($TiCl_3$ only for d)) mononuclear species on the $MgCl_2$ (110) surface. EB adsorbs a) directly onto the $TiCl_4$ species, b) at the nearest Mg^{2+}, c) at the adjacent layer, and d) directly onto the $TiCl_3$ species.

sterically important ligand position in the 3-sites model,[6,7]

c) adsorption of EB on the neighboring $MgCl_2$ layer, which must be the farest position for EB to affect the stereospecifity of the Ti center.[12]

Similar three coadsorption states were considered for the coadsorption of the $TiCl_3$ mononuclear species and EB. Note that EB was directly attached to the most stable 5f intra-layer0 species without a structural transformation (Figure 4d).

On the (100) surface, four typical coadsorption states of EB and $TiCl_4$ were shown in Figure 5a-d:

a) direct attachment of EB onto the $TiCl_4$ species, where $TiCl_4$ was transformed into an O_h bridging species,

b) adsorption of EB at the 5-fold coordinated Mg^{2+} ion nearest to the $TiCl_4$ species,

c)-d) adsorption of EB on the neighboring $MgCl_2$ layer with its molecular plane perpendicular and parallel to the layer, respectively.

Again, the corresponding four states were considered in the case of $TiCl_3$, and the direct EB adsorption onto $TiCl_3$ was done without a structural transformation of $TiCl_3$ (Figure 5e).

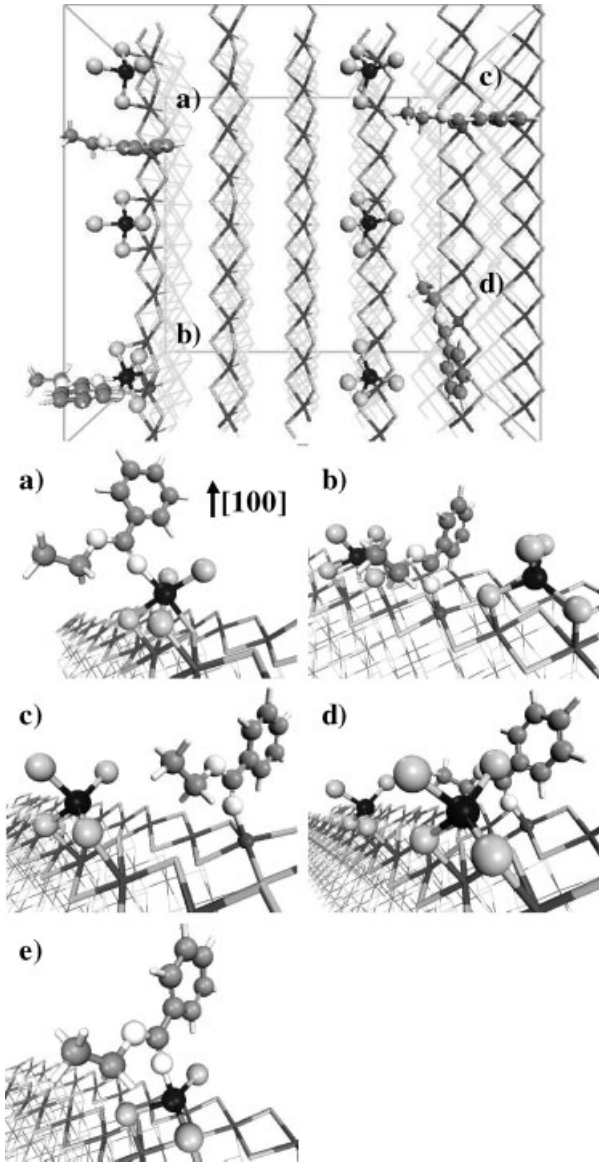

Figure 5.
Typical coadsorption states of EB and $TiCl_4$ mononuclear species on the $MgCl_2$ (100) surface. EB adsorbs a) directly onto the $TiCl_4$ species, b) at the nearest Mg^{2+}, c)-d) at the adjacent layer with its molecular axis, respectively, perpendicular and parallel to the layer, and e) directly onto the $TiCl_3$ species.

Defining the coadsorption energy (E_{coad}) as the total adsorption energy of the coadsrobed system {E_{ad} (Ti species + EB)} *minus* the sum of the two adsorption energies of the separate adsorbants {E_{ad} (Ti species) + E_{ad} (EB)}, Table 2 summarizes E_{coad} of the coadsorption states and charge distributions among the Ti species, EB and support for the (110) and (100) surfaces.

The direct adsorption of EB to the $TiCl_4$ species on the (110) surface was 25.17 kcal/mol less advantageous than the separate adsorption, owing to the breakment of the O_h symmetry of $TiCl_4$. That on the (100)

Table 2.
Coadsorption states of the $TiCl_x$ mononuclear species and EB on the $MgCl_2$ (110) and (100) surfaces.

species	position of EB	E_{coad}[a)]/kcal · mol^{-1}	charge			C=O/nm
			$TiCl_x$	$MgCl_2$	EB	
$TiCl_4$ on (110)	$TiCl_4$	25.17	−0.241	−0.014	0.256	0.1247
	nearest Mg^{2+}	6.38	−0.160	0.106	0.056	0.1243
	adjacent layer	−0.37	−0.136	0.028	0.110	0.1241
$TiCl_3$ on (110)	$TiCl_3$	−2.33	−0.225	0.027	0.201	0.1250
	nearest Mg^{2+}	1.73	−0.185	0.091	0.097	0.1245
	adjacent layer	−3.18	−0.188	0.059	0.131	0.1242
$TiCl_4$ on (100)	$TiCl_4$	10.51	−0.189	−0.120	0.312	0.1259
	nearest Mg^{2+}	2.44	0.062	−0.119	0.061	0.1245
	adjacent layer$_\perp$[b)]	5.46	0.078	−0.151	0.075	0.1247
	adjacent layer$_{//}$[b)]	4.38	0.072	−0.177	0.108	0.1241
$TiCl_3$ on (100)	$TiCl_3$	−0.25	−0.080	−0.150	0.233	0.1255
	nearest Mg^{2+}	2.51	−0.009	−0.057	0.070	0.1245
	adjacent layer$_\perp$[b)]	5.46	0.012	−0.086	0.079	0.1247
	adjacent layer$_{//}$[b)]	6.36	0.021	−0.123	0.106	0.1242

[a)] E_{coad} is the differential energy between the total adsorption energy of the coadsorbed system and the sum of the two adsorption energies of the separate adsorbants.
[b)] // and ⊥ subscripts indicate the direction of the molecular axis of EB.

surface was also much less stable. In addition, $\{E_{ad}$ (Ti species) $+ E_{ad}$ (EB)$\}$ was below −40 kcal/mol, while the complexation energy of $TiCl_4 \cdot EB$ was calculated as −16.18 kcal/mol. Namely, the complex between EB and $TiCl_4$ is likely to dissociate on the $MgCl_2$ support, unless all surface Mg^{2+} ions are occupied. This inferance seems consistent with our previous experimental results with thermal analysis and IR, where various catalysts prepared by, for example, cogrinding the $TiCl_4 \cdot EB$ complex with $MgCl_2$ or reacting pre-cogrineded EB/$MgCl_2$ with $TiCl_4$, led to the dominance of the separate adsorbands with the resudual amount of the complex on the support.[26] On the contrary, the EB-$TiCl_3$ species was as stable as the separate adsorption on both the surfaces, where the C=O distances was elongated through the back-donation by ca. 0.003 nm from the gas-phase value. For the adsorption of EB at the Mg^{2+} ions close to the $TiCl_4$ or $TiCl_3$ species, E_{coad} were only $-3.18 \sim +6.38$ kcal/mol on the (110) surface (but tended to be smaller (more stable) for the less bulky $TiCl_3$), and were slightly positive, $+2.44 \sim +6.36$ kcal/mol, on the (100) surface. Thus, it seemed that there was no preferential plancement between the Ti species and EB on the $MgCl_2$ surfaces, *i.e.* the placement of the two adsorbants should be decided in a random way at typical reaction temperatures, and therefore effects of the coadsorption on polymerization behaviours be dependent on the surface coverage.

For the charge distribution among the Ti species, EB ions and support, the following results were obtained.

a) For the direct adsorption of EB to the Ti species, the charge transfer occured only between the Ti species and EB, and the charge of the support became almost neutral on the (110) surface (Table 2). On the contrary, EB donated its electron both directly to the Ti species and indirectly to the support via the Ti species on the (100) surface (Table 2). The order of the electron richness of the Ti species (with EB) was $TiCl_4$ on (110) $>$ $TiCl_3$ on (110) $>$ $TiCl_4$ on (100) $\gg$ $TiCl_3$ on (100).
b) For the coadsorption of EB to the surrounding Mg^{2+} ions, both EB and the support more or less donated their electron to the Ti species on the (110) surface, resulting in the enhanced electron density of the Ti species (compared with that of the separate adsorption). On the (100) surface, both the $TiCl_4$

species and EB released their electron towards the support, while the charge of the $TiCl_3$ species was rarely affected by the coadsorption with EB.

In this way, the electronic interplay among the three components completely differed on the two types of the surfaces. Concentrating on the coadsorption of EB at the surrounding Mg^{2+} ions, the electron density of the Ti species was increased on the (110) surface, indicative of the enhanced back-donation from the Ti center to monomer, *i.e.* higher reactivity for monomer insertion. On the other hand, the coadsorption of EB did not show any positive electronic effect for the reactivity of the Ti species on the (100) surface. This electron-enriched Ti species on the (110) surface might explain the donor-related highly active and stereoselective Ti species proposed by Sacchi et al.[4] and Liu et al.[7]

Conclusion

A series of the periodic density functional calculations was firstly excuted in order to grasp a microscopic image for the interplay among the Ti species, EB and $MgCl_2$. We showed that the relative placement between the $TiCl_4$ or $TiCl_3$ species and EB should be decided randomly on both the $MgCl_2$ (110) and (100) surfaces, and that the electron density of the Ti species was increased by EB only on the (110) surface. The latter finding suggests that the role of the coadsorbed EB is dependent on the type of the $MgCl_2$ planes and more important on the (110) surface.

Acknowledgements: This work was supported by TOHO CATALYST Co., LTD.

[1] [1a] Belgian Patent 785 332, Montedison; [1b] Belgian Patent 785 334, Montedison.
[2] E. Albizzati, U. Giannini, G. Collina, L. Noristi, L. Resconi, *Propylene Handbook*, E. P. Moore, Ed., Hanser, New York **1996**, Chapter 2.
[3] P. C. Barbé, G. Cecchin, L. Noristi, *Adv. Polym. Sci.* **1986**, *81*, 1.
[4] M. C. Sacchi, I. Tritto, P. Locatelli, *Prog. Polym. Sci.* **1991**, *16*, 331.
[5] V. Busico, P. Corradini, L. De Martino, A. Proto, V. Savino, *Makromol. Chem.* **1985**, *186*, 1279.
[6] [6a] V. Busico, R. Cipullo, G. Monaco, G. Talarico, M. Vacatello, *Macromolecules* **1999**, *32*, 4173;[6b] P. Corradini, V. Barone, R. Fusco, G. Guerra, *J. Catal.* **1982**, *77*, 32.
[7] B. Liu, T. Nitta, H. Nakatani, M. Terano, *Macromol. Chem. Phys.* **2003**, *204*, 395.
[8] M. C. Sacchi, I. Tritto, P. Locatelli, *Eur. Polym. J.* **1988**, *24*, 137.
[9] J. V. Seppälä, M. Härkönen, *Makromol. Chem.* **1989**, *190*, 2535.
[10] K. K. Kang, T. Shiono, Y.-T. Jeong, D.-H. Lee, *J. Appl. Polym. Sci.* **1999**, *71*, 293.
[11] M. Toto, G. Morini, G. Guerra, P. Corradini, L. Cavallo, *Macromolecules* **2000**, *33*, 1134.
[12] L. Barino, R. Scordamaglia, *Macromol. Theory Simul.* **1998**, *7*, 407.
[13] M. Boero, M. Parrinello, H. Weiss, S. Hüffer, *J. Phys. Chem. A* **2001**, *105*, 5096.
[14] M. Seth, T. Ziegler, *Macromolecules* **2003**, *36*, 6613.
[15] S. Yao, Y. Tanaka, *Macromol. Theory Simul.* **2001**, *10*, 850.
[16] J. P. Perdew, K. Burke, M. Ernzerhof, *Phys. Rev. Lett.* **1996**, *77*, 3865.
[17] K. Labonowski, J. Andzelm, Eds. *Density Functional Methods in Chemistry*, Springer-Verlag, New York **1991**.
[18] [18a] M. Dolg, U. Wedig, H. Stoll, H. Preuss, *J. Chem. Phys.* **1987**, *86*, 866;[18b] A. Bergner, M. Dolg, W. Kuechle, H. Stoll, H. Preuss, *Mol. Phys.* **1993**, *80*, 1431.
[19] B. Delley, *J. Phys. Chem.* **1990**, *92*, 508.
[20] T. Taniike, M. Terano, *Macromol. Rapid. Commun.* submitted.
[21] F. L. Hirshfeld, *Theory Chim. Acta B* **1977**, *44*, 129.
[22] E. Magni, G. A. Somorjai, *J. Phys. Chem. B* **1998**, *102*, 8788.
[23] [23a] J. D. Gale, C. Richard, A. Catlow, M. J. Gillan, *Top. Catal.* **1999**, *9*, 235;[23b] G. Monaco, M. Toto, G. Guerra, P. Corradini, L. Cavallo, *Macromolecules* **2000**, *33*, 8953;[23c] M. Seth, P. M. Margl, T. Ziegler, *Macromolecules* **2002**, *35*, 7815.
[24] M. Boero, M. Parrinello, K. Terakura, *J. Am. Chem. Soc.* **1998**, *120*, 2746.
[25] J. C. W. Chien, L. C. Dickinson, J. Vizzini, *J. Polym. Sci. A.* **1990**, *28*, 2321.
[26] M. Terano, T. Kataoka, *Makromol. Chem., Macromol. Chem. Phys.* **1987**, *188*, 1477.

